Flow regimes of unsteady laminar flow past a slender elliptic cylinder at incidence

Jin Koo Park, Seung O. Park, Jae Min Hyun
Department of Mechanical Engineering, Korea Advanced Institute of Science and Technology, Chong Ryang, Seoul, Korea

The effect of incidence on the unsteady laminar flow past an impulsively started, slender elliptic cylinder was studied numerically for the Reynolds numbers ranging between 25 and 600. The DuFort–Frankel scheme and the Buneman algorithm were adopted to solve the system of governing equations in stream-function–vorticity formulation. As a result of the present numerical experiment, we identified five distinct flow regimes: two regimes of steady flow and three regimes of unsteady flow. The two steady flow regimes were demarcated by the presence of a steady separation bubble. The boundary between the two steady regimes was well represented by a simple empirical formula. The three unsteady flow regimes were characterized by the frequency and amplitude of the periodic variations of force coefficients. These five regimes were mapped out in the incidence–Reynolds number plane. The details of flow characteristics pertinent to the respective flow regime are discussed.

Keywords: unsteady laminar flow; elliptic cylinder; unsteady flow regime; Strouhal number

Introduction

The characteristics of two-dimensional flows behind bluff bodies, in particular, behind circular cylinders, have been extensively investigated by many authors. In the case of a circular cylinder, it is well known that if the Reynolds number is in the range 3–6, the flow separates from the cylinder and a pair of attached vortices form behind the cylinder. A further increase of the Reynolds number above 30–45 leads to an oscillation of the wake, and the wake eventually develops to the well documented Karman vortex street.[1,2]

No systematic investigation, however, of the unsteady flow patterns of the laminar flow past an elliptic cylinder at incidence over a wide range of the Reynolds numbers has been reported yet. Evidently, it is anticipated that there are considerable similarities between the flow past an elliptic cylinder and the flow past a circular cylinder. Several research results have been published for low Reynolds number flows past an inclined elliptic cylinder, for example, Hasimoto,[3] Tomotika and Aoi,[4] Imai,[5] and Shintani *et al.*[6] The early stage of unsteady flow past an elliptic cylinder at zero degree incidence has been studied by Richards,[7] and Dennis and Chang,[8] Wang[9] and Staniforth[10] investigated theoretically the separation and stall in the developing stages of the flow around an impulsively started elliptic cylinder. Taneda[11] conducted experiments to ascertain the relation between the lift and the separation of an impulsively started elliptic cylinder at incidences of 20° and 45°. Honji[12] performed experiments to delineate the flow pattern around an impulsively started elliptic cylinder at various incidences using flow visualization techniques for the Reynolds numbers in the range between 50 and 600. Three different cylinders were used in his work, each having the thickness to chord ratio of 33.3%, 50%, and 55%. He dealt with only the initial stage of unsteady flow. It was pointed out that the initial formation of a wake bubble behind the near side of the elliptic cylinder was considerably affected by the incidence. The laminar flows past an elliptic cylinder at 45° incidence for the Reynolds numbers of 15, 30 and 200 were studied numerically by Lugt and Haussling.[13] In that study, steady state solutions were found for the Reynolds numbers of 15 and 30. However, when the Reynolds number was 200, the well-known Karman vortex street was observed. Recently, Patel[14] adopted the series truncation method to solve the stream function and vorticity equations for the flow past an elliptic cylinder at 0°, 30°, 45°, and 90° incidence. The Reynolds numbers considered in his work were 100 and 200.

A survey of the previous literature indicated that the flow pattern has been studied only for a small number of discrete values of incidence. Results of previous studies also suggest that the flow characteristics are altered considerably when the incidence varies. As has been mentioned earlier, no systematic and comprehensive investigation has been reported to single out the question of how the flow structure changes when the variation of the incidence is minute. In order to address this problem, a large number of flow calculations are necessary using very small increments of the angle of incidence. It is expected that the incidence will be a vital parameter to determine the transitory behavior as the flow transforms from the well-established steady-state solutions to the Karman vortex street. We intend, in this study, to characterize the change of flow patterns as the incidence varies for a given Reynolds number. Further, we attempt to construct a regime diagram which demonstrates the character of transitory flow past an elliptic cylinder in the incidence–Reynolds number plane.

Numerical details

Governing equations and boundary conditions

For an effective depiction of the flow past an elliptic cylinder at incidence, we employ an elliptic coordinate system as

Address reprint requests to Dr. Hyun at the Department of Mechanical Engineering, Korea Advanced Institute of Science and Technology, P.O. Box 150, Chong Ryang, Seoul, Korea.

Received 11 July 1988; accepted 20 January 1989

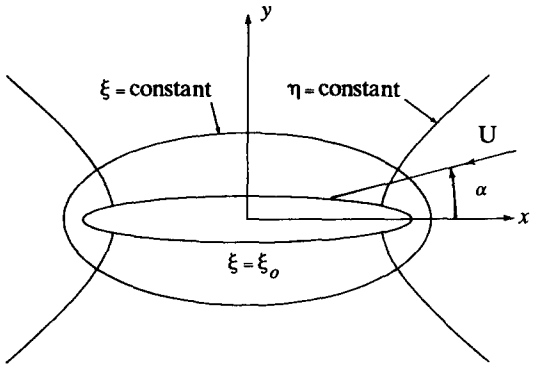

Figure 1 Elliptic coordinate system

sketched in Figure 1. The coordinate transformation from x-y plane to ξ-η plane is defined by

$$x+iy=c\cosh(\xi+i\eta) \qquad c>0 \tag{1}$$

The chord length of the elliptic cylinder is given by

$$l=2c\cosh\xi_0 \tag{2}$$

where ξ_0 is the ξ-coordinate at the surface of the cylinder.

The nondimensional governing equations formulated in terms of stream function, and vorticity, in ξ and η coordinates can be written as[13,14]

$$\frac{\partial\omega}{\partial t}+\frac{1}{J}\frac{\partial(\omega,\psi)}{\partial(\xi,\eta)}=\frac{L}{\mathrm{Re}}\left\{\frac{1}{J}\left(\frac{\partial^2\omega}{\partial\xi^2}+\frac{\partial^2\omega}{\partial\eta^2}\right)\right\} \tag{3}$$

and

$$\frac{1}{J}\left\{\frac{\partial^2\psi}{\partial\xi^2}+\frac{\partial^2\psi}{\partial\eta^2}\right\}=\omega \tag{4}$$

Here,

$$J=h^2=\cosh^2\xi-\cos^2\eta \tag{5}$$

$$L=\frac{l}{c}=2\cosh\xi_0 \tag{6}$$

The dimensionless velocity components in terms of stream function, are expressed as

$$u_\xi=\frac{1}{h}\frac{\partial\psi}{\partial\eta} \tag{7a}$$

$$u_\eta=-\frac{1}{h}\frac{\partial\psi}{\partial\xi} \tag{7b}$$

Along the surface of the cylinder, the no-slip condition is applied, for $t>0$:

$$\psi=\frac{\partial\psi}{\partial\xi}=0 \qquad \text{at } \xi=\xi_0 \tag{8}$$

Far from the cylinder, the potential flow solution will be recovered. Thus, the boundary condition there is written as

$$\frac{\partial\psi}{\partial\xi}=-e^{\xi_0}\cosh(\xi-\xi_0)\sin(\eta-\alpha) \qquad \text{as } \xi\to\infty \tag{9}$$

The initial condition for the impulsively starting flow can be given by the following potential flow field:

$$\psi=-e^{\xi_0}\sinh(\xi-\xi_0)\sin(\eta-\alpha) \tag{10}$$

Numerical methods

The governing equations described in the previous section were integrated in a finite domain. Since our aim was to characterize the flow patterns for various combinations of the Reynolds number and the incidence, a large number of numerical calculations had to be carried out. For the present calculation, the incidence was varied from 0 to 90° with a minimum increment of 2.5° for a fixed Reynolds number. The elliptic cylinder adopted for the present investigation was defined by $\xi_0=0.15$, which gave the chord length of 2.023 and the thickness to chord ratio of 14.89%.

The DuFort–Frankel scheme was used to solve the vorticity transport equation (Equation 3). The Buneman algorithm with first variant (see Buzbee *et al.*[15]) was employed to solve the stream function equation (Equation 4). Since the Buneman algorithm is a direct method to solve the Poisson's equation, it was necessary to examine the solutions afterward. When the accuracy of the solutions was not satisfactory, the successive line overrelaxation (SLOR) was subsequently used until the solution attained the desired accuracy. This procedure reduced substantially the computational time required to solve the stream function equation. The five-point approximate formula of Equation 4 was solved by the Buneman algorithm with cyclic odd/even reduction normal to the ξ-direction. Next, the accuracy of its solution was checked by the residual $|\nabla^2\psi-\omega|$ at each grid point. For the present calculation, the accuracy was considered to be sufficient when the maximum of the residual was less than 10^{-4}. If the above criterion was not met, we subsequently employed SLOR to solve Equation 4, using the solution of the Buneman algorithm as an initial guess, until the desired accuracy was attained. With the single precision mode of IBM 3083JX, the residuals were of the order of 10^{-3}–10^{-5}. However, with the double precision mode of the same machine, the residuals were always less than 10^{-4}. Therefore, the SLOR procedure was unnecessary for this case.

Notation

c	Focal distance
C	Coefficient in transformed Equation 12
C_L	Lift coefficient
J, h^2	Jacobian
l	Chord length
l_s, l_t	Characteristic lengths in streamwise and transverse direction, respectively
L	Dimensionless chord length, l/c
n	Frequency of oscillation
Re	Reynolds number, Ul/ν
S_t	Strouhal number, ln/U
t	Dimensionless time
t	Thickness of elliptic cylinder
U	Free stream velocity
u_ξ, u_η	Dimensionless velocity in ξ and η direction, respectively
x, y	Cartesian coordinates
x_∞	x-coordinate of the outer boundary at $y=0$
y_∞	y-coordinate of the outer boundary at $x=0$
α	Incidence
ν	Kinematic viscosity
ω	Vorticity
ψ	Stream function
ξ, η	Elliptic coordinates

The allowable time step, Δt, for the DuFort–Frankel scheme was determined as follows. The modified equation of the DuFort–Frankel scheme for Equation 3 becomes[16]

$$\frac{\partial \omega}{\partial t}+C\frac{\partial^2 \omega}{\partial t^2}+\frac{1}{J}\frac{\partial(\omega,\psi)}{\partial(\xi,\eta)}=\frac{L}{\mathrm{Re}}\left\{\frac{1}{J}\left(\frac{\partial^2 \omega}{\partial \xi^2}+\frac{\partial^2 \omega}{\partial \eta^2}\right)\right\} +O(\Delta t^2, \Delta \xi^2, \Delta \eta^2) \tag{11}$$

where

$$C=\frac{L}{\mathrm{Re}\,J}(\Delta t)^2\left\{\frac{1}{(\Delta \xi)^2}+\frac{1}{(\Delta \eta)^2}\right\} \tag{12}$$

For the consistency of the solution, it is necessary that the coefficient C be very small. For a given value of C, Δt can be obtained as

$$\Delta t_{\max}=\left[\frac{C\,\mathrm{Re}\,J_{\min}}{L(1/\Delta \xi^2+1/\Delta \eta^2)}\right]^{1/2} \tag{13}$$

Here, $J_{\min}$ is the minimum value of J over all grid points. For the present calculation, C was given the value of 0.001–0.004. In order to resolve the rapid changes of the initial flow field after the impulsive starting, actual time steps were given much smaller values than that given by Equation 13. The first time step was set to be one-tenth of $\Delta t_{\max}$ given by Equation 13. After the first time step was advanced, Δt was gradually increased to the final value of $\Delta t_{\max}$ over some specified time interval, t_s, which was prescribed beforehand.

Other specifics, such as the grid spacings ($\Delta \xi$ and $\Delta \eta$), the number of grid points, the length of the outer boundary measured from the major axis of the elliptic cylinder, the prescribed time interval, t_s, and the final time, t_f, for the calculations performed in the present work, are listed in Table 1. As explicitly expressed in Table 1, the sizes of the calculation domains were taken to be sufficiently large (see the values of x_∞/l and y_∞/l).

Since the computational domain was finite, the boundary condition at infinity prescribed by Equation 9 could not be strictly implemented. The boundary condition of Equation 9 was applied only on the upstream half of the outer boundary. On the downstream half of the outer boundary, the convection of vorticity and momentum across the border with free stream velocity was imposed. At the body surface a one-sided second-order difference scheme[13] was employed to calculate the vorticity. For the details of the finite difference approximations for Equations 3 and 4, and of the boundary conditions, see Lugt and Haussling.[13]

Results and discussion

For the flow past an elliptic cylinder at incidence, the geometrical asymmetry brings about considerable changes in the flow characteristics. Both the separation phenomena and the free shear layer development in the wake are very sensitive to changes of incidence. Inspection of the essential data, i.e., the streamlines, equivorticity lines, C_L-curves, enabled us to delineate five regimes of distinct flow characteristics which are sketched in Figure 2. The characteristics of the flows in these regimes will be discussed in detail.

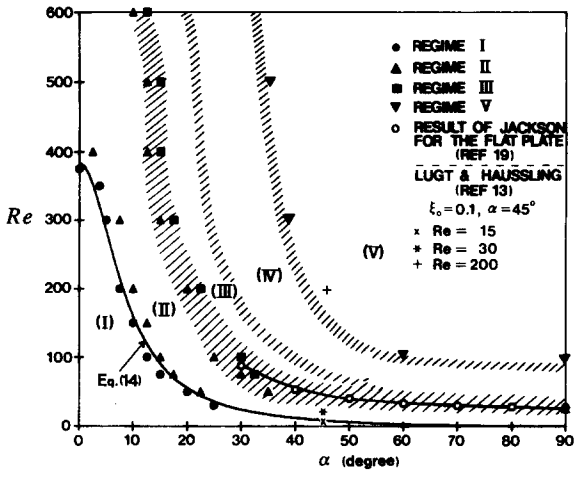

Figure 2 Flow domain map

Steady flow regimes: regimes I and II

For the flows in regimes I and II, almost steady-state solutions were obtained. The distinction between regime I and II was necessary to identify the existence of a separation bubble; flows in regime I did not possess any separation bubble, while those in regime II had a separation bubble over the surface. Since there was no separation bubble in regime I flow, one attachment line near the leading edge and a separation line in the vicinity of the trailing edge characterized the streamline pattern. Steady-state solutions were approached monotonically from the corresponding initial inviscid solutions in regime I. The streamlines, from some distance downstream, were quite straight and parallel to the main flow direction. The corresponding vorticity contour indicated that the positive and negative vorticities merely spread downstream in a symmetrical manner. This suggested that the wake was stable in regime I flow.

When the angle of incidence was further increased from that of a flow in regime I, the flow pattern with a separation bubble (regime II flow) appeared. As mentioned previously, the presence of a separation bubble and the steadiness of the flow at large times are the salient features of regime II flows. Typical streamline patterns and vorticity contours are displayed in Figure 3. In the region adjacent to regime I (i.e., region of lower incidence in regime II), the flow establishment toward steady state was monotonic. However, in the region close to regime III (i.e., region of higher incidence in regime II), steady state was reached in an oscillatory manner. In the former case, the steady-state separation bubble emerged monotonically. However, in the latter case, the steady-state separation bubble appeared after a cycle of "opening" or "bursting" of an incipient separation bubble. The transient behavior of flow in this regime was well described by Lugt and Haussling, and hence it is not repeated here. The computational results for the flows past an

Table 1 The list of parameters used in the calculation

α	$N_\xi \times N_\eta$	$\Delta\xi \times \Delta\eta$	x_∞/l	y_∞/l	t_s	t_f
$0 \le \alpha \le 10$	84 × 128	0.04 × 0.0491	7.952	7.937	1.0	15–30
$10 < \alpha \le 30$	90 × 64	0.04 × 0.0982	10.106	10.094	1.5	30–60
$30 < \alpha \le 60$	95 × 64	0.04 × 0.0982	12.341	12.331	2.0	30–60
$60 < \alpha \le 90$	98 × 64	0.04 × 0.0982	13.913	13.904	2.5	30–45

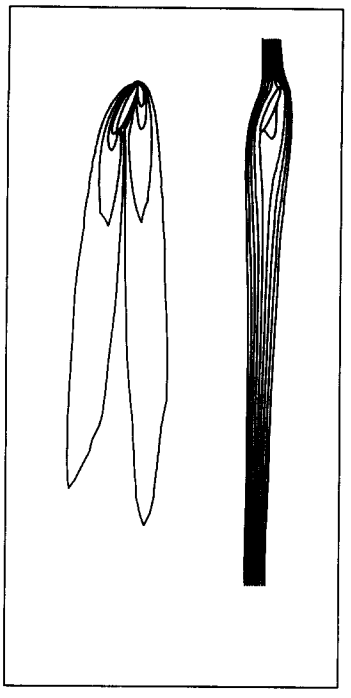

Figure 3 Streamlines and equi-vorticity lines for Re = 100, $\alpha = 22.5°$ at $t = 30$

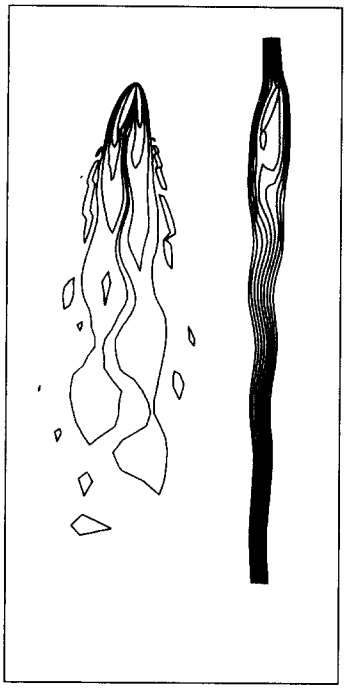

Figure 4 Streamlines and equi-vorticity lines for Re = 300, $\alpha = 20°$ at $t = 30$

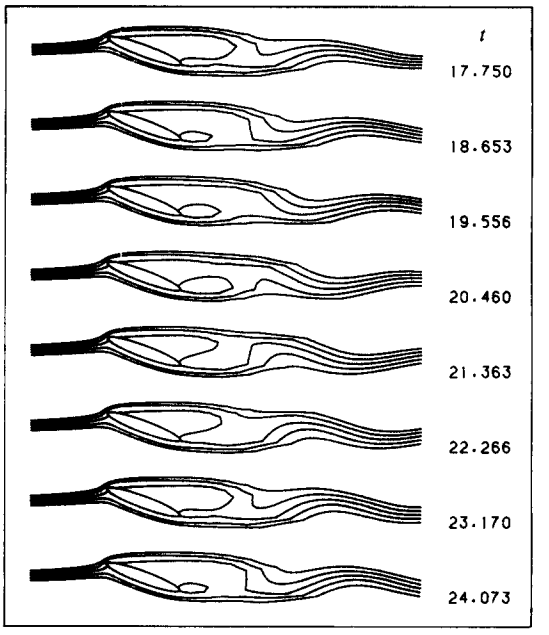

Figure 5 The sequential development of streamlines with time for Re = 300, $\alpha = 20°$

elliptic cylinder for the case of Re = 15 and $\alpha = 45°$ and of Re = 30 and $\alpha = 45°$ by Lugt and Haussling did reveal the monotonic approach and oscillatory approach to steady state, respectively.

The boundary between regimes I and II can be closely approximated by

$$\mathrm{Re} = \gamma \left(\frac{l_s}{l_t} \right)^2 \tag{14}$$

where l_s and l_t are the characteristic lengths in the streamwise and transverse direction, respectively, and γ is an empirical constant. Since regime I and regime II are distinguished by the presence of a separation bubble, Equation 14 was conceived based on the speculation that the flow in regime I is dominantly influenced by the diffusion of vorticity. When an elliptic cylinder at incidence is considered, two distinct lengths, that is, the transverse length, l_t, and the streamwise length, l_s may characterize the flow configuration. The Reynolds number is the single dynamic similarity parameter, as is well known. The ratio of diffusive terms will be like $(l_s/l_t)^2$. This simple-minded dimensional analysis resulted in Equation 14. The lengths l_s and l_t are given by

$$l_s^2 = l^2 \cos^2 \alpha + t^2 \sin^2 \alpha \tag{15a}$$

$$l_t^2 = l^2 \sin^2 \alpha + t^2 \cos^2 \alpha \tag{15b}$$

where t is the thickness of the elliptic cylinder.

When the constant γ was chosen to be 8.5, the boundary between regime I and II was very closely traced, as shown in Figure 2. For the case of circular cylinder, where $l_s = l_t$, Equation 14 gives the critical Reynolds number of 8.5. It is reminded that the critical Reynolds number for a circular cylinder, at which twin vortices start to appear, is about 6.[1] Equation 14 also implies that, when an elliptic cylinder is normal to the free stream, the critical Reynolds number decreases as the ellipse becomes thinner, as pointed out by Batchelor.[2]

Flow regimes with oscillating wakes: regions III, IV, and V

When the incidence angle increases beyond the limit within which the flow exhibits a steady and stable character, the flow becomes unsteady; the streamlines in the wake become wavy and the forces acting on the cylinder become periodic. The unsteady flow regime can further be divided into three subregimes. We designate these three subregimes as regime III, IV, and V, respectively (see Figure 2). The flow characteristics in these regimes are discussed next. Flow in regime III (Figure 2) is typified by the streamlines and vorticity contours exemplified in Figure 4. The streamline pattern continuously undergoes a periodic change. The sequence of instantaneous streamline patterns exhibited in Figure 5 demonstrates this character. Note that a separation bubble is formed alternately. The alternate formation of a separation bubble is accompanied by the formation of the instantaneous "alleyways" of fluid (see Perry *et al.*[17]). Streamlines of a flow in this flow regime from some downstream distance appear to be sinusoidal (Figure 4). However, the amplitude of the sinusoidal streamlines is much smaller than that of the streamlines of regime IV or V flows. Presumably, the flow situation in regime III is analogous to that of the unsteady flow regime categorized as the *incipient Karman range* by Morkovin[18] of the flow past a circular cylinder. Recently, Jackson[19] computed the critical Reynolds numbers for various bodies at which the transition from steady to periodic flow occurs by locating a Hopf bifurcation point. The results of Jackson for a flat plate was about 27.8. In our case of the elliptic cylinder, it was about 25. Also, it is noted that the critical Reynolds number for the flat plate at 30° incidence lies very close to that for the present case of the elliptic cylinder. These observations point to the belief that the solid line between regime II and III represents the locus of Hopf bifurcation point for the slender elliptic cylinder under present investigation.

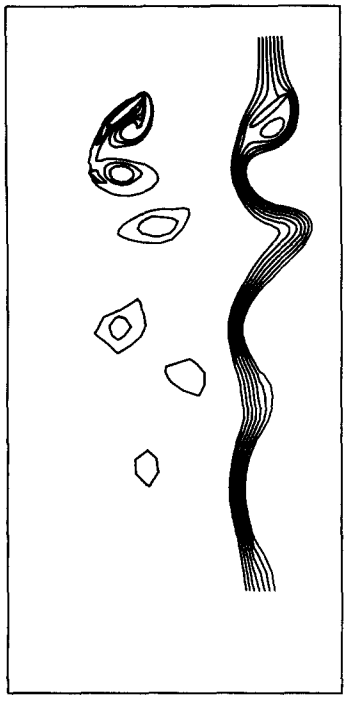

Figure 6 Streamlines and equivorticity lines for Re = 300, $\alpha = 50°$ at $t = 30$

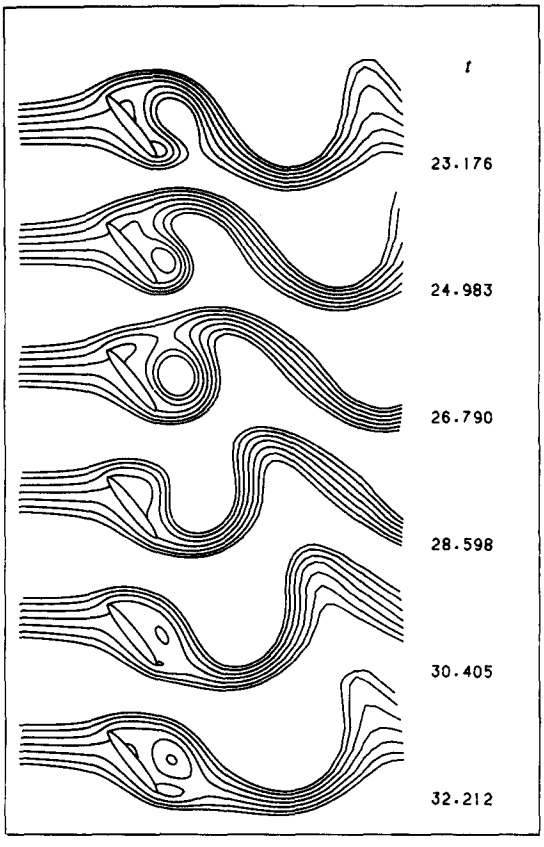

Figure 7 The sequential development of streamlines with time for Re = 300, $\alpha = 50°$

As the incidence increases, the undulation of streamlines in the wake became more pronounced. The conspicuous undulation of streamlines is obviously a result of the formation of discrete vortex cores in the wake. Examination of the vorticity contours revealed that the discrete vortices emerge at a much shorter distance from the trailing edge when the incidence is increased. As an illustration, the streamlines and equivorticity lines for the case of $\alpha = 50°$ and Re = 300 are exhibited in Figure 6. The case presented in Figure 6 corresponds to a flow in regime V. As seen from the figure, the undulation of streamlines in regime V is far more complex. Streamlines at some typical instants are displayed in Figure 7. The leading-edge separation bubble and the trailing-edge separation bubble shed alternately in the wake as discrete vortices. Usually, a secondary bubble is induced about the mid-chord by the roll-up of a strong vortex in the vicinity of the cylinder. Later, this secondary bubble grows and is merged with the trailing edge bubble. The growth of separation bubbles and their shedding into the wake are responsible for the large amplitude in periodic variations of the C_L-curve. The frequency of oscillation of C_L-curves in regime V was found to be much lower compared to that of regime III flows. The periodic variation of streamlines and C_L-curve suggests that the regime V flows correspond to the pure Karman range of Morkovin. The distinct characteristic differences between regimes III and V were unaffected by the size of the calculation domain as was used in the present computations.

The regime IV flow is intermediate between regime III and V flows; the boundary band between these two regimes is referred to as regime IV. In this intermediate regime there appear two dominant frequencies in the C_L-curves. A high-frequency oscillation mode was superposed on a low-frequency mode. The intermediate nature of oscillation in regime IV flows is clearly visible in Figure 8, where the C_L-curves for the three unsteady regimes are compared. To delineate the frequency characteristics of the unsteady flow regimes, a finite Fourier analysis of the C_L-curves was carried out. The results are contained in Figure 9. It is seen that the dominant frequency

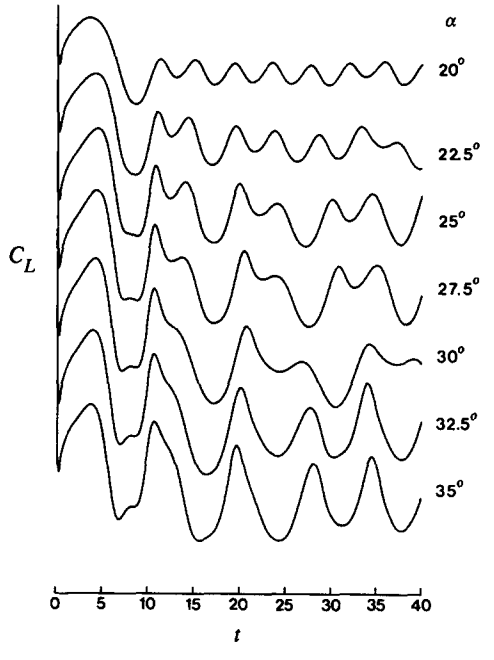

Figure 8 The variation of C_L-curves with time at various incidences (Re = 500)

of regime III flow ($\alpha = 20°$) is about twice as high as that of regime V flow ($\alpha = 35°$). In regime IV flows, two dominant frequency peaks are present. Also, the gradual migration of energy from the higher frequency mode to the lower frequency one is noticeable.

The degree of interaction between the near surface flow and the wake can be illustrated by the movement of singular points (i.e., zero shear stress points) over the surface. Such an illustration is provided in Figure 10. It is noticed that the movement of a singular point near the leading edge is rather insensitive to the change of incidence, while the other singular points are very sensitive. The amplitude of the periodic variation of the singular points of regime III flow (Figure 10) is seen to be much smaller than that of regime V flow (Figure 10). Again, regime IV flows exhibit intermediate properties (Figures 10(b) and (c)). The movement of singular points depicted in the figure demonstrates that the interaction between the near surface flow and the wake becomes stronger as the incidence is increased. This tendency can also be realized in the C_L-curves, which merely reflect the pressure distribution and the skin friction around the surface of the cylinder (see Figure 8).

The boundaries confining regime IV flows were very difficult to pinpoint. Thus, in the regime diagram of Figure 2, those were marked by a broader, shaded band. However, the existence of an intermediate region (which is fairly wide) between the incipient Karman range and the pure Karman range is a very unique feature in the flow past an elliptic cylinder at incidence. So far, the existence of such a region has not yet been fully appreciated, especially, in the case of a circular cylinder.

Since there are two dominant frequencies in regime IV flows, the Strouhal number in this regime is somewhat obscure to define. Thus, in Figure 11, where the variation of the Strouhal number with the incidence is presented, the curves corresponding to regime IV flows are marked by shaded dashed lines. It is noted that the Strouhal number decreases with the incidence for a given Reynolds number. More importantly, the increase of the Strouhal number with the Reynolds number is apparent only in regime III flows. The dependence of the Strouhal number on the Reynolds number is virtually negligible in regime V flows, at least in the present range of investigation. Also shown in the figure is a critical Strouhal number curve plotted from Jackson's data for a flat plate. It is seen that the Strouhal numbers for the present elliptic cylinder are larger than those for the case of a flat plate.

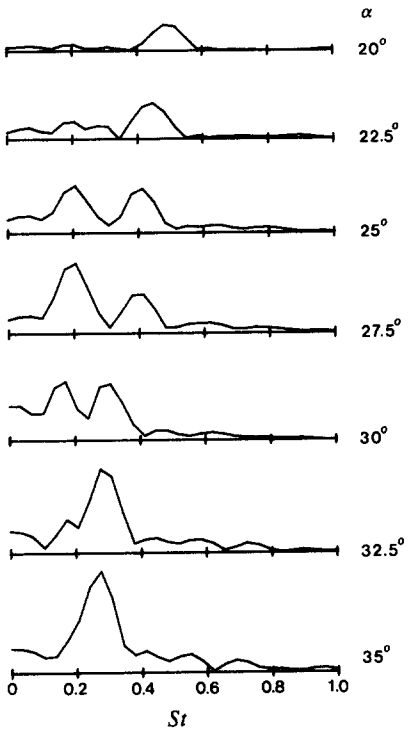

Figure 9 The power spectra of C_L-curves at various incidences (Re=500)

Conclusion

A systematic numerical experiment was performed to investigate the details of the laminar unsteady flows past an elliptic cylinder

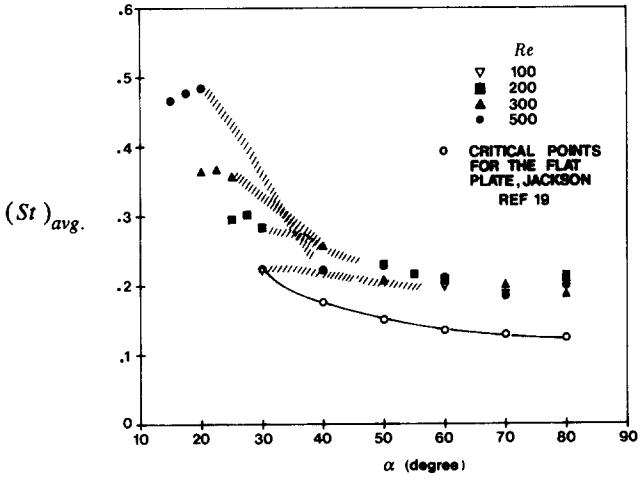

Figure 11 The variation of Strouhal number with incidence

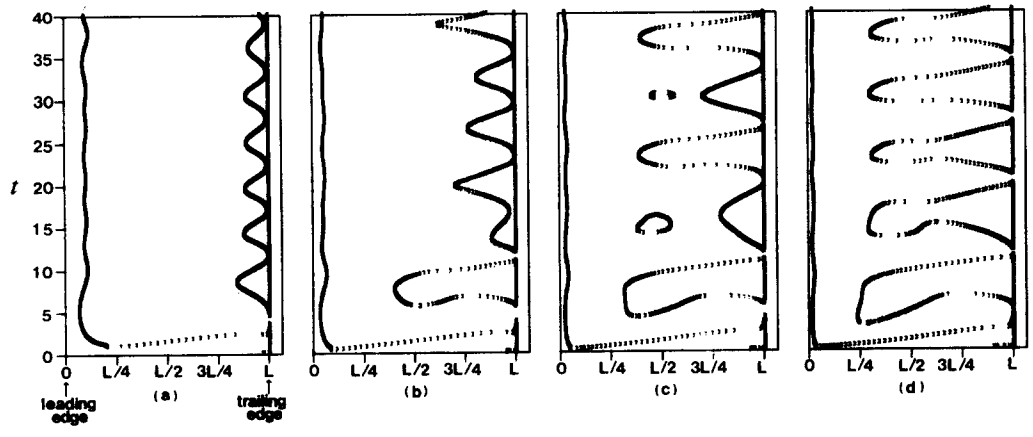

Figure 10 The movement of singular points on the surface with time at various incidences for Re=300: (a) $\alpha=22.5°$; (b) $\alpha=27.5°$; (c) $\alpha=32.5°$; (d) $\alpha=37.5°$

at incidence. Five regimes of distinguished flow characteristics were identified. Steady flow region could be divided into two regimes. The streamline pattern in one regime (regime I) was characterized by a reattachment point and a separation point, which did not possess any separation bubble. The other steady flow regime (regime II) was characterized by the existence of a separation bubble. The critical Reynolds number signaling the appearance of a separation bubble was well represented by the square of the transverse to longitudinal characteristic length ratio.

The boundary between the steady flow regime and the unsteady one could be viewed as the locus of Hopf bifurcation point. The unsteady flow region could further be classified into three regimes. The first regime (regime III) corresponded to the incipient Karman range and another one (regime V) to the pure Karman range. The third one (regime IV) was an intermediate regime between these two. The shedding frequency of regime III was about twice as high as that of regime V. Regime IV flows were found to have two discrete characteristic frequencies. The Strouhal number was found to depend strongly on the Reynolds number only in the incipient Karman range (regime III) for the present case of elliptic cylinder.

References

1 Taneda, S. Experimental investigation of the wakes behind cylinders and plates at low Reynolds numbers. *Journal of Physical Society of Japan*, 1956, **11**, 302

2 Batchelor, G. K. *An Introduction to Fluid Dynamics*. Cambridge University Press, Cambridge, 1967

3 Hasimoto, H. On the flow of a viscous fluid past an inclined elliptic cylinder at small Reynolds numbers. *Journal of Physical Society of Japan*, 1953, **8**, 653

4 Tomotika, S. and Aoi, T. The steady flow of a viscous fluid past an elliptic cylinder and a flat plate at small Reynolds numbers. *Quarterly Journal of Mechanics and Applied Mathematics*, 1953, **6**, 290

5 Imai, I. A new method of solving Oseen's equations and its application to the flow past an inclined elliptic cylinder. *Proceedings of the Royal Society of London A*, 1954, **224**, 141

6 Shintani, K., Umemura, A., and Takano, A. Low-Reynolds-number flow past an elliptic cylinder. *Journal of Fluid Mechanics*, 1983, **136**, 277

7 Richards, G. J. On the motion of an elliptic cylinder through a viscous fluid. *Philosophical Transactions of the Royal Society of London A*, 1934, **233**, 279

8 Dennis, S. C. R. and Chang, G. Z. Numerical investigation of the Navier-Stokes equations for steady two-dimensional flow. *The Physics of Fluids Supplement II*, 1969, **12**, II88

9 Wang, C. Y. Separation and stall of an impulsively started elliptic cylinder. *Journal of Applied Mechanics*, 1967, **34**, 823

10 Staniforth, A. N. Studies of symmetrical and asymmetrical viscous flow past impulsively started cylinder. Ph.D. Thesis, University of Western Ontario, 1972

11 Taneda, S. The development of the lift of an impulsively started elliptic cylinder at incidence. *Journal of Physical Society of Japan*, 1972, **33**, 1706

12 Honji, H. Starting flows past spheres and elliptic cylinders. *Reports of Research Institute for Applied Mechanics*, Kyushu University, 1972, **19**, 271

13 Lugt, H. J. and Haussling, H. J. Laminar flow past an abruptly accelerated elliptic cylinder at 45° incidence. *Journal of Fluid Mechanics*, 1974, **65**, 711

14 Patel, V. A. Flow around the impulsively started elliptic cylinder at various angles of attack. *Computers and Fluids*, 1981, **9**, 435

15 Buzbee, B. L., Golub, G. H., and Nielson, C. W. On the direct methods for solving Poisson's equations. *SIAM Journal of Numerical Analysis*, 1970, **7**, 672

16 Roache, P. *Computational Fluid Dynamics*. Hermosa, Albuquerque, 1972

17 Perry, A. E., Chong, M. S., and Lim, T. T. The vortex shedding process behind two-dimensional bluff bodies. *Journal of Fluid Mechanics*, 1982, **116**, 77

18 Morkovin, M. V. Flow around circular cylinder—a kaleidoscope of challenging fluid phenomena. *Symposium on Fully Separated Flows*, ed. Hansen, A. G. ASME, 1964, 102

19 Jackson, C. P. A finite-element study of the onset of vortex shedding in flow past variously shaped bodies. *Journal of Fluid Mechanics*, 1987, **182**, 23